

Article

The Influence of Absorbing Coating Material on the Efficiency of Laser Shock Peening

Elena Gachegova ^{1,*}, Denis Davydov ^{2,3}, Sergey Mironov ⁴, Alexander Kalinenko ⁴, Maxim Ozerov ⁴, Sergey Zharebtsov ^{4,5} and Oleg Plekhov ¹

¹ Institute of Continuous Media Mechanics, Ural Branch of Russian Academy of Science, Ak. Koroleva Str. 1, 614013 Perm, Russia; poa@icmm.ru

² M.N. Mikheev Institute of Metal Physics, Ural Branch of Russian Academy of Science, S. Kovalevskaya Str. 18, 620108 Ekaterinburg, Russia

³ Department of Natural Sciences, Ural State University of Railway Transport, Kolmogorova St. 66, 620034 Ekaterinburg, Russia

⁴ Laboratory of Bulk Nanostructured Materials, Belgorod State University, Pobedy Str. 85, 308015 Belgorod, Russia; mironov@bsu.edu.ru (S.M.); kalinenko@bsu.edu.ru (A.K.); ozerov@bsu.edu.ru (M.O.)

⁵ World-Class Research Center, Advanced Digital Technologies, Saint-Petersburg Marine Technical University, Lotsmanskaya Str. 3, 190121 Saint-Petersburg, Russia

* Correspondence: gachegova.e@icmm.ru

Abstract: Laser shock peening (LSP) is a relatively novel and promising surface hardening method. An absorbing layer, which is needed to protect the specimen surface from undesirable thermal effects caused by laser irradiation, should be considered as one of many varying parameters. The physical characteristics of the coating and its adhesion to the specimen surface can significantly influence the result of LSP. In this study, three commonly used absorbing coatings, namely black polyvinylchloride tape with a sticky layer, aluminum foil, and black alkyd paint were used to cover three-millimeter-thick plates of the Ti-6Al-4V titanium alloy with globular or lamellar microstructures. LSP of one side of the plates was carried out with a power density of 10 GW/cm². The hole drilling method was used to evaluate residual stresses. The aluminum foil was found to be the optimal option for LSP of the Ti-6Al-4V titanium alloy. Microstructural investigations carried out using EBSD analysis suggested that no significant reduction in grain size, twinning, or dislocation density growth occurred as a result of LSP irrespective of the initial structure.

Keywords: laser shock peening; residual stress; microstructure



Citation: Gachegova, E.; Davydov, D.; Mironov, S.; Kalinenko, A.; Ozerov, M.; Zharebtsov, S.; Plekhov, O. The Influence of Absorbing Coating Material on the Efficiency of Laser Shock Peening. *Metals* **2024**, *14*, 1045. <https://doi.org/10.3390/met14091045>

Academic Editor: Belén Díaz Fernández

Received: 25 July 2024

Revised: 4 September 2024

Accepted: 6 September 2024

Published: 13 September 2024



Copyright: © 2024 by the authors. Licensee MDPI, Basel, Switzerland. This article is an open access article distributed under the terms and conditions of the Creative Commons Attribution (CC BY) license (<https://creativecommons.org/licenses/by/4.0/>).

1. Introduction

Laser shock peening (LSP) is currently considered to be one of the most promising and effective methods of surface treatment for metallic materials. Deep compressive residual stresses created due to this treatment improves fatigue properties and corrosion resistance, thereby increasing machine parts performance [1]. The formation of compressive residual stresses in the near-surface layer of the material up to two millimeters in depth is a result of the propagation of a short pressure pulse caused by the process of interaction of laser radiation with the substance. In order to protect the treated surface against the direct impact of laser radiation, a coating (these coatings are often referred to as absorbing, protective, or as a sacrificial layer) can be used.

Additionally, a confining layer (water or glass) is usually applied to increase the pressure of the expanding plasma [2] due to restraining hydrodynamic dispersion of the plasma formed on the material surface. During LSP, a laser beam passing through the confining layer is absorbed by the protective coating or the specimen surface, thereby producing plasma which is enclosed between the surface and confining layer. The pressure exerted on the material surface by the expanding confined plasma creates a stress wave

that propagates into the material. If the amplitude of the wave is large enough, the material begins to deform plastically, which in turn leads to the creation of a residual stress field. The propagation of plastic deformation caused by the elastic–plastic wave continues until the maximum stress value decreases below the dynamic yield strength of the material. The scheme of the laser shock peening process is shown in Figure 1.

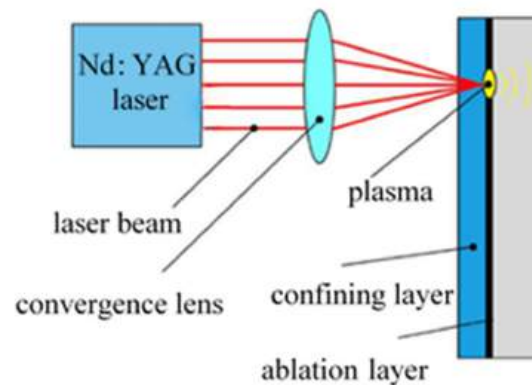


Figure 1. Schematic diagram of laser shock peening.

The following materials can be used for coating: aluminum foil 80–100 microns thick [3–5], polyvinyl chloride tape 40 microns thick (hereinafter referred to as PVC tape) [6], and organic black paint [7]. Another way to carry out LSP is the uncoated (i.e., without using of any sacrificed layer) treatment [8–11]. To date, no studies have been conducted to compare the performance of all traditional coatings on the same material under identical LSP conditions.

This study aimed therefore to examine the effect of different absorbing coatings on the efficiency of LSP under identical loading conditions. The residual stress profiles were utilized as a measure of the LSP efficiency.

One of the most prevalent alloys utilized in the aerospace industry, Ti-6Al-4V, was used as the program material. Titanium alloys are employed primarily in structures that require a combination of high specific strength and corrosion resistance, such as fan and compressor blades of gas turbine engines, for which high fatigue strength and durability are critical performance characteristics.

In this work, a comprehensive study of the processes accompanying laser shock peening was conducted by investigating the microstructure and microhardness of the specimens after treatment. Unlike residual stresses and fatigue characteristics, the microstructural aspect of laser shock peening of titanium alloy Ti-6Al-4V has attracted less attention. Nevertheless, several recent studies have provided valuable information on the microstructural processes induced by laser shock peening. In particular, the formation of a nanocrystalline structure [12–16] and even amorphization [17] have been observed in a narrow surface layer. However, beneath this layer, microstructural changes are usually much less pronounced. An increase in dislocation density is often observed in both the α [16,18–21] and β [16,22] phases. Shear bands can also be observed occasionally [22]. Of particular interest was the detection of mechanical twinning in the α phase [14–17,20,23], despite the fact that this mechanism is generally believed to be not quite typical for Ti-6Al-4V.

Although significant progress has been made in previous microstructural studies, the literature data are very inconsistent. In this regard, this work investigated the microstructural changes in Ti-6Al-4V after LSP. For a more complete analysis of the physical mechanisms responsible for the formation of residual stresses, a comparative analysis of the changes in the microstructure of the material depending on the initial state of the material was carried out for lamellar and globular microstructures. The microstructural analysis was conducted using orientation microscopy (or electron backscattered diffraction (EBSD) analysis) [23–25].

2. Materials and Methods

2.1. Laser Shock Peening and Material

A Nd:YAG laser with a wavelength of 1064 nm and a pulse duration of 10 ns was employed to treat the surface of plate-like specimens with a side of 40 mm and a thickness of 3 mm. The treatment was conducted on one side of the plates. The processing parameters are presented in Table 1.

Table 1. Parameters of laser shock peening.

Parameter	Value
Power density	10 GW/cm ²
Geometry of the laser beam spot	Square with 1 mm side
Overlap	0%
Pulse frequency	5 Hz
Size of the treatment area	30 × 30 mm

Three types of coatings were investigated as an absorbing layer: 80 µm thick aluminum foil, black alkyd paint (layer thickness 40 µm), and 100 µm thick black PVC tape. Additionally, an uncoated treatment was considered.

In the initial condition, the alloy had a globular or a lamellar microstructure that were used to establish the effect of microstructure on residual stress generation. The program Ti-6Al-4V titanium alloy with a globular microstructure material was supplied in the form of a bar produced by hot rolling. A lamellar microstructure was obtained by annealing at 1010 °C for 15 min and subsequent air cooling.

2.2. Microstructural Studies

LSP plates with different initial microstructures were sectioned through the middle of the treated area. Then, after sectioning, the samples were mounted into a conductive phenolic thermoplastic resin with a KonductoMet™ graphite filler using a Buehler SimpliMet™ 4000 (Lake Bluff, IL, USA) hot press at 170 °C and 160 bar for 90 s with further cooling at room temperature for 5 min.

The obtained tablets were ground and polished using LaboPol-5 and Struers devices (Paris, France), respectively. An abrasive paper with gradual reduction in abrasivity down to P2000 (the abrasive particle size is 7 microns) was used. To prevent overheating of the samples, water was supplied to the grinding wheel. After mechanical grinding, the samples were polished using diamond suspensions with particle sizes of 6, 3, and 1 µm on a MD-Nap velvet cloth. The final polishing was performed using a Buehler VibroMet™ 2 vibration polishing machine (Lake Bluff, IL, USA) and OP-S colloidal silicon suspension for extended time intervals (up to 24 h).

The EBSD analysis was performed using an FEI Quanta 600 (Lausanne, Switzerland) scanning electron microscope at an accelerating voltage of 20 kV and a beam size of 6. The aperture diameter for imaging was 50 µm and the working distance was 15 mm. The scanning step for macro imaging (i.e., overview map) was 1 or 2 µm. For high-resolution imaging of the microstructure in the LSP region, the scanning step was 0.1 or 0.2 µm. In order to minimize the error, at least 7 Kikuchi lines were determined. The average value of the coefficient characterizing the correctness of the automatic indication of the Kikuchi maps (the so-called “confidence index”, CI [20]) exceeded 0.1 (in this case, the value of correctly indicated electronograms should exceed 95% [20]). Grains comprising two or fewer pixels were subjected to cleaning using the TSL OIM Analysis 8 program (Berwyn, PA, USA). Due to the limited angular resolution of the EBSD method, boundaries exhibiting disorientation of less than 2° were excluded from consideration. Boundaries with disorientation between 2° and 15° were considered low-angle boundaries (LAGs), and boundaries with disorientation above 15° were considered high-angle boundaries (HAGs).

Two specific EBSD characteristics were used for microstructural analysis, namely the Image Quality Index (Image Quality (IQ)) and the Kernel Average Misorientation (KAM).

2.3. Residual Stress Measurement

The residual stresses were quantified using the hole drilling method [26], which was implemented with an automated MTS3000-Restan machine. The measurement procedure involved drilling a hole with a diameter of 2 mm, which altered the initial deformation state, facilitating the redistribution of the residual stresses generated in the material during LSP. The current strains were quantified using a specially configured three-element strain gauge socket, after which they were utilized to calculate [27] the residual stresses using the specialized EVAL 8 software (Calenzano, Italy), developed by SINT Technology. The measurement procedure includes the following steps. The strain gauge is mounted on the specimen using adhesive. A through or blind hole is drilled through the geometric center of the socket of this sensor layer-by-layer. In each layer, the deformations resulting from the removal of the residual stresses are recorded. The residual stresses were then calculated using special calculation algorithms [27].

In the case of non-uniform stresses, the surface strain unload, measured after completion of the hole depth step j depended on the residual stresses that were initially present in the material at all hole depth steps $1 \leq k \leq j$:

$$\varepsilon_j = \frac{1+\nu}{E} \sum_{k=1}^j a_{jk} \left(\frac{(\sigma_x)_k + (\sigma_y)_k}{2} \right)_k + \frac{1}{E} \sum_{k=1}^j b_{jk} \left(\frac{(\sigma_x)_k - (\sigma_y)_k}{2} \right)_k \cos 2\theta + \frac{1}{E} \sum_{k=1}^j b_{jk} (\tau_{xy})_k \sin 2\theta \quad (1)$$

where $(\sigma_x)_k$ is the normal stress in the x -direction, $(\sigma_y)_k$ is the normal stress in the y -direction, $(\tau_{xy})_k$ is the shear stress in the xy plane, E is Young's modulus, ν is Poisson's ratio, a_{jk} and b_{jk} are calibration coefficients obtained by the finite element method (FEM), and θ is the orientation angle of each strain gauge [28].

In this work, type A strain gauges manufactured by TML were utilized, enabling the residual stresses to be measured at a depth of up to 1 mm.

All measurements were performed in accordance with ASTM E 837-13, "Standard Test Method for Determining Residual Stresses by Hole Drilling Using a Strain Gauge" [26].

2.4. Microhardness Measurement

The samples for microhardness measurements were cut using an electrical discharge machine with minimal power to eliminate the thermal influence of the spark on the layer obtained as a result of LSP. The measurements were carried out using a METOLAB 502 microhardness tester (Moscow, Russia) [29]. The series of measurements were carried out in the planes parallel to the treated surface with a step of 0.1 mm (11 series in total). The distance from the surface for the first series was 2 diagonals of the print, about 0.05 mm. In each series (10 measurements) the step along the plane, parallel to the surface, was 0.2 mm. The load was 10 N.

3. Results

3.1. Initial State

Titanium alloy Ti-6Al-4V is an industrial alloy and belongs to the group of alloys with a two-phase ($\alpha + \beta$) structure [30]. Figure 2 depicts typical EBSD maps of the alloy in the initial globular state. It can be observed that the microstructure is homogeneous, entirely globular, with an average diameter of the alpha phase particles of approximately 10 μm .

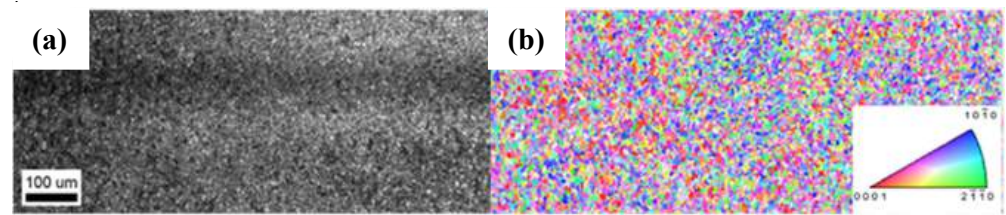


Figure 2. EBSD maps of the program material with globular microstructure: (a) IQ map, (b) orientation map.

The EBSD map obtained from the initial material with a lamellar microstructure is shown in Figure 3. The map reveals a hierarchical microstructure consisting of very coarse (~ 1 mm) initial (transformed) beta grains, large (~ 100 μm) alpha colonies, and alternating alpha and beta phase plates within the colonies.

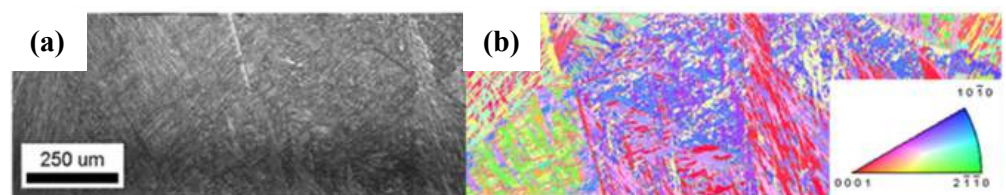


Figure 3. EBSD maps of source material with lamellar microstructure: (a) IQ map, (b) orientation map.

3.2. Structural Studies

Taking into account the results of the previous paragraphs, for structural studies the treatment was carried out using a protective layer of aluminum foil.

The EBSD overview map obtained from the specimen with an initially lamellar microstructure after LSP is presented in Figure 4.



Figure 4. Overview EBSD IQ map of the initial material with lamellar microstructure after LSP (the surface is at the top of the micrograph).

To gain further insight into the microstructural changes induced by LSP, a high-resolution EBSD map was obtained (Figure 5). As can be seen from the IQ map, no significant changes in the morphology and size of the alpha plates were observed (Figure 5a). Additionally, no plate reversal in the direction of the preferential plastic flow of the metal, which usually occurs in the deformation of plate structures, was detected (Figure 5a). Moreover, the IQ and KAM maps did not even show a significant change in contrast, thus exhibiting no clear evidence of an increase in dislocation density (Figure 5a,b). Also, the orientation map (Figure 5c) showed no signs of the formation of either small-angle boundaries of deformation origin or twins.

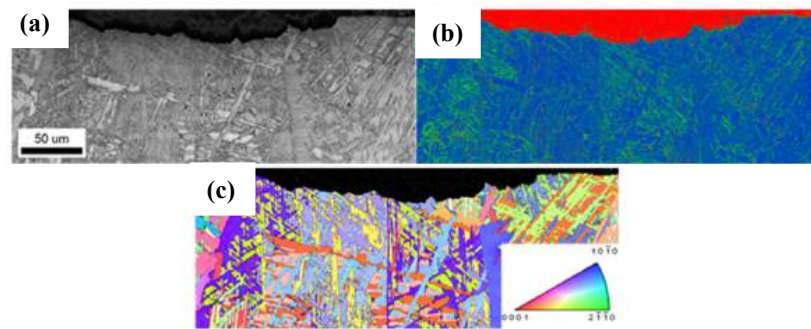


Figure 5. High-resolution EBSD maps of the material with an initially lamellar structure after LSP: (a) IQ map, (b) KAM map, and (c) orientation map. In fragment (c), the light and dark lines correspond to the small-angle and large-angle boundaries. The surface is at the top of the micrograph.

An overview map of EBSD obtained for a specimen with an initially globular microstructure after its surface treatment is shown in Figure 6.

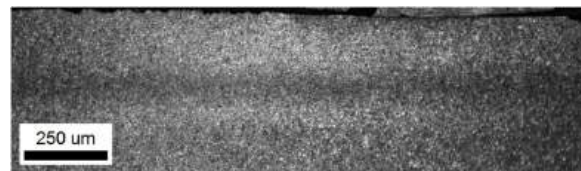


Figure 6. Overview EBSD IQ map of the initial material with globular microstructure after LSP (the surface is at the top of the micrograph).

For a more detailed study of microstructural changes induced by laser shock peening, a high-resolution EBSD map was obtained (Figure 7). As can be seen from the IQ map, there are no changes in the size or the shape of the grains, particularly their flattening, in the alpha phase, (Figure 7a). However, this map shows some darkening of the contrast (Figure 7a), which can be interpreted as an increase in the overall density of lattice dislocations. In contrast, the KAM map does not show any significant anomalies (Figure 7b). This observation can be explained as follows. The dislocations in metallic materials can be broadly categorized into two groups, viz., geometrically necessary ones and statistically stored ones [31]. The geometrically necessary dislocations produce orientation gradients, and thus they may give rise to a contrast in the KAM maps. On the other hand, the statistically stored dislocations result only in the degradation of the crystal lattice structure (thereby becoming visible in the IQ maps) but provide no orientation gradients. In view of the above issues, the experimental observations in the present work can be attributed to an accumulation of the statistically stored dislocations. The orientation map (Figure 7c) did also not indicate the formation of either small-angle boundaries of deformation origin or twins.

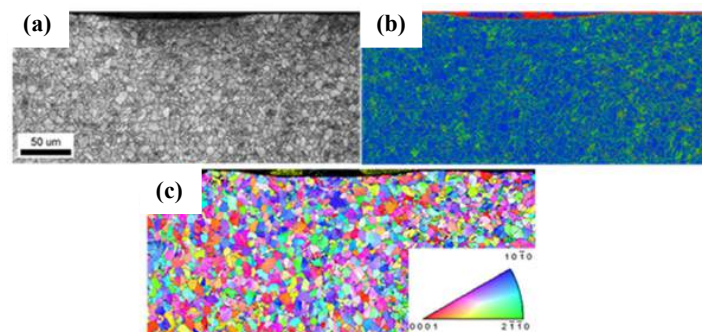


Figure 7. High-resolution EBSD maps of the material's surfaces with an initially globular structure: (a) IQ map, (b), KAM map, and (c) orientation map. In fragment (c), the light and dark lines correspond to small-angle and large-angle boundaries. The surface is at the top of the micrograph.

3.3. Measurements of Residual Stresses and Coating Effects

The application of the protective coatings serves to prevent thermal damage to the specimen surface (Figure 8a), which is readily apparent in the absence of an absorbing layer (Figure 8b).

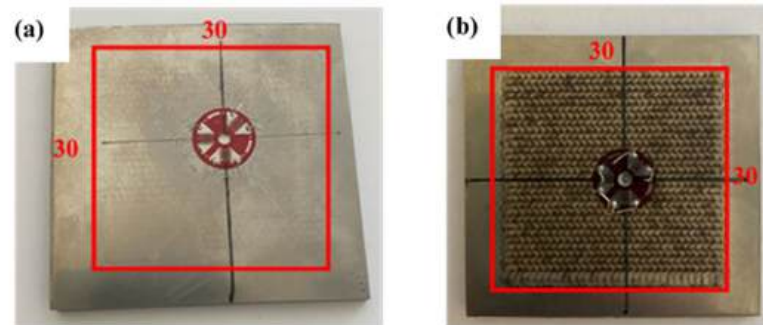


Figure 8. The specimens treated with an absorbing coating (a) and without an absorbing coating (thermal damage by laser radiation is visible on the surface of the processed zone) (b). The specimens are equipped with a strain gauge to measure the residual stresses.

Figure 9 shows the outcomes of the residual stress measurements (Figure 9a,b) across the depth of the specimen in the center of the processed area, for distinct initial microstructures of the specimens (Figure 9a,b). Despite the differences in the thermal treatment of the material and significantly different microstructures (lamellar (Figure 3a) and globular (Figure 2b)), LSP with a protective layer of metal foil did not exhibit a significant alteration in the residual stresses.

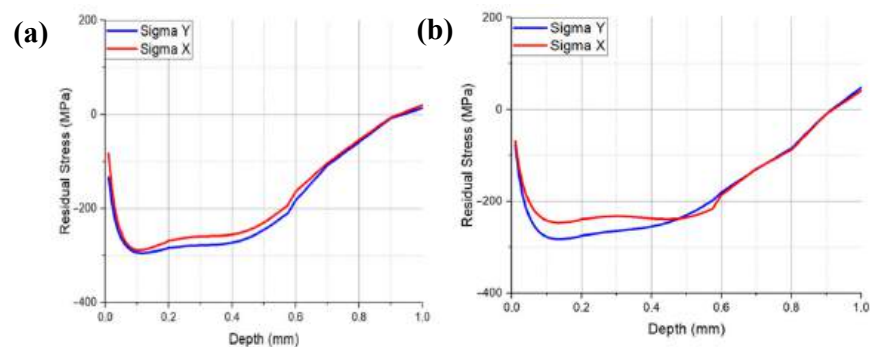


Figure 9. Profiles of residual stress components in the plane of treatment by depth for the lamellar (a) and globular (b) conditions of the alloy.

The initial microstructure exerts no qualitative influence on the distribution of residual stresses in the specimen. That is why further investigation of the effect of protective coatings on the distribution of residual stresses in specimens was focused on the alloy with the globular microstructure.

Figure 10 illustrates the residual stress profiles for distinct protective coatings subjected to LSP with a power density of 10 GW/cm^2 . The specimen coated with black paint exhibited the greatest compressive residual stress, with a value of -400 MPa along the X-axis, while the highest value of the hardened layer depth was achieved in the case of treatment with aluminum foil. Upon examination of the depth of compressive residual stresses across all specimens, it becomes evident that there is minimal variation, with the exception of the aluminum foil specimen in the X-axis direction. However, the maximum value of compressive stress exhibits a notable discrepancy. This is particularly evident in the case of the vinyl tape specimen, where the compressive stress reaches only -130 MPa .

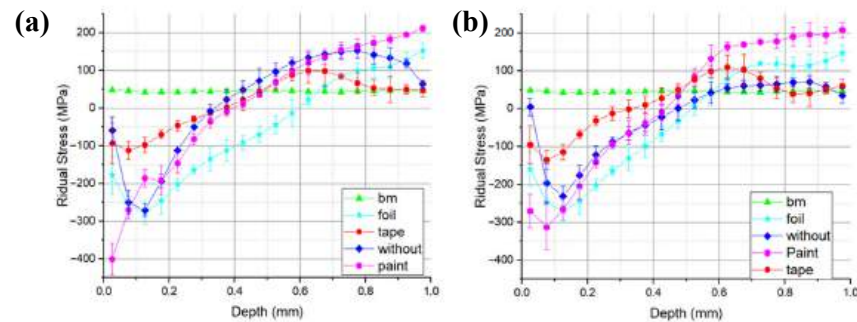


Figure 10. Depth profiles of residual stresses in the Ti-6Al-4V alloy with the globular microstructure: (a) stresses along the X-axis; (b) stresses along the Y-axis.

It is also important to note that the material of the absorbing coating has a significant effect on the residual stresses on the surface of the specimen. These residual stresses play an important role in improving the fatigue properties of the material. The residual stress profiles obtained for the specimen covered with PVC tape and the uncoated one demonstrate that the residual stresses on the surface do not exceed -100 MPa. In contrast, aluminum foil and black paint on the surface result in values of -180 MPa and -400 MPa, respectively.

When evaluating the integral values of residual stresses averaged over the entire treatment layer, it was also found that the use of aluminum foil is the most effective treatment mode with a value of -50.92 MPa \cdot mm, whereas in the case of black paint, this value is 32.08 MPa \cdot mm, with tape it is 17.64 MPa \cdot mm, and without an absorbing layer it is 22.37 MPa \cdot mm. The observed reduction in integral values for all types of protective coating, with the exception of aluminum foil, can be attributed to the presence of significant tensile stresses (up to 200 MPa) at a depth of 0.4 mm. In the case of foil, this depth is approximately 0.6 mm.

The obtained result can be corroborated by estimating the maximum plasma pressure and the fraction of energy that will be reflected when using different types of absorbing coating. Following the methodology outlined in [32], we estimated the peak plasma pressure using the limited ablation mode hypothesis as:

$$P(\text{GPa}) = \sqrt{\frac{\alpha}{2\alpha + 3}} \sqrt{Z} \sqrt{I_0} \quad (2)$$

where α is the energy fraction for plasma formation (0.25 – 0.4), I_0 —power density of laser radiation, and Z —acoustic impedance between the absorbing limiting layer:

$$\frac{2}{Z} = \frac{1}{Z_{\text{coat}}} + \frac{1}{Z_{\text{H}_2\text{O}}} \quad (3)$$

Using the acoustic impedance values for water, titanium, vinyl tape, aluminum, and paint: $Z(\text{H}_2\text{O}) = 0.15 \cdot 10^6$ g/cm 2 s $^{-1}$, $Z(\text{Ti}) = 2.2 \cdot 10^6$ g/cm 2 s $^{-1}$, $Z(\text{Al}) = 1.45 \cdot 10^6$ g/cm 2 s $^{-1}$, $Z(\text{Tape}) = 0.25 \cdot 10^6$ g/cm 2 s $^{-1}$, $Z(\text{Paint}) = 1.5 \cdot 10^6$ g/cm 2 s $^{-1}$ we obtained the following values of Z :

$$\begin{aligned} Z(\text{H}_2\text{O} + \text{Ti}) &= 0.28 \cdot 10^6 \text{ g/cm}^2 \text{ s}^{-1} \text{ (without coating),} \\ Z(\text{H}_2\text{O} + \text{Al}) &= 0.27 \cdot 10^6 \text{ g/cm}^2 \text{ s}^{-1}, \\ Z(\text{H}_2\text{O} + \text{Tape}) &= 0.18 \cdot 10^6 \text{ g/cm}^2 \text{ s}^{-1}, \\ Z(\text{H}_2\text{O} + \text{Paint}) &= 0.27 \cdot 10^6 \text{ g/cm}^2 \text{ s}^{-1}. \end{aligned} \quad (4)$$

The relations (4) indicated that aluminum foil, uncoated treatment, and paint permit the acquisition of almost identical pressure pulses, whereas the pulse amplitude with vinyl

tape on the surface is approximately 20% lower. The evaluation of the pressure pulse at an energy density of 10 GW/cm² gave the following peak pressures:

$$\begin{aligned} P(\text{Ti}) &= 4.5 \text{ GPa}, \\ P(\text{Al}) &= 4.4 \text{ GPa}, \\ P(\text{Tape}) &= 3.6 \text{ GPa}, \\ P(\text{Paint}) &= 4.4 \text{ GPa}. \end{aligned}$$

Another crucial process influencing the efficacy of the treatment was the reflection of the elastic–plastic wave at the interface between the protective coating and the specimen. If there is a significant difference in acoustic impedance between the absorbing layer and the sample material at the interface, a significant part of the energy can be reflected. To estimate the proportion of the passed energy, the values of the energy transmittance D_{en} and the amplitude transmittance D_{amp} were:

$$D_{en} = \left(\frac{2 Z_{coat.}}{Z_{coat.} + Z_{sp.}} \right)^2 \quad (5)$$

$$D_{amp} = \frac{2 Z_{coat.}}{Z_{coat.} + Z_{sp.}} \quad (6)$$

The calculation of the parameters gave the following values:

$$\begin{aligned} D_{en}(\text{Ti} + \text{Al}) &= 0.891, \\ D_{en}(\text{Ti} + \text{Tape}) &= 0.451, \\ D_{en}(\text{Ti} + \text{Paint}) &= 0.900; \end{aligned} \quad (7)$$

$$\begin{aligned} D_{amp}(\text{Ti} + \text{Al}) &= 0.794, \\ D_{amp}(\text{Ti} + \text{Tape}) &= 0.204, \\ D_{amp}(\text{Ti} + \text{Paint}) &= 0.810. \end{aligned} \quad (8)$$

The analysis of the relations (7) and (8) indicated that the use of aluminum foil or black paint results in a 10% loss of energy at the coating–specimen boundary, which corresponded to almost a 20% loss of pulse amplitude. The PVC tape–specimen boundary is essentially impermeable to the wave resulting in the loss of up to 80% of the pulse amplitude. From a technological standpoint, aluminum foil offers a distinct advantage in terms of application speed and can be effectively utilized for parts with simple geometries. However, when dealing with small curvature radii and intricate geometries, there is a potential risk of loss of adhesion between the foil and the part, which could result in the tearing of the protective layer or the formation of defects on the surface of the material in the area of non-continuities at the boundary of the protective layer. In this instance, the application of paint is a more suitable option, although it necessitates a considerably longer application time to achieve the required thickness of the protective layer.

3.4. Measurement of Microhardness after Laser Shock Treatment

The microhardness of the material was weakly dependent on the physical nature of the protective layer material. Figure 11 shows the depth dependence of microhardness in the Ti-6Al-4V alloy with the globular microstructure for all investigated coating materials. The change in microhardness is most significant in the case of treatment with vinyl tape, where the peak of microhardness reached a value of 350 HV. The modes without coating and with paint gave very similar results both in terms of microhardness distribution profile and its values.

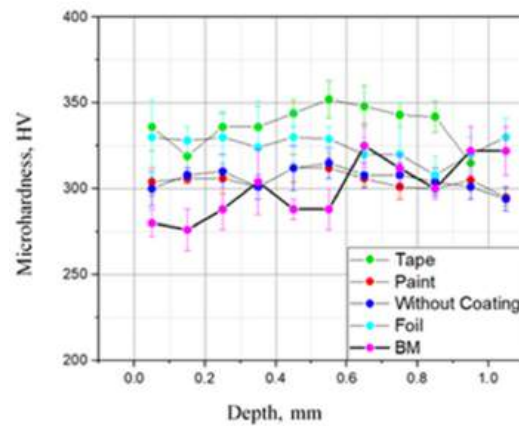


Figure 11. Curves of microhardness dependence on depth in the Ti-6Al-4V alloy with the globular microstructure.

4. Conclusions

In this paper we studied the influence of different absorbing coatings on the efficiency of laser shock peening on the Ti-6Al-4V titanium alloy. Flat specimens were treated from one side with power density of 10 GW/cm^2 . The analysis of residual stress profiles obtained after processing led to the formulation of the following conclusions.

All used coatings withstood processing with an energy density of 10 GW/cm^2 , maintaining their integrity, and can be used in industry.

The residual stress profiles indicated that the use of aluminum foil and black paint is the most effective. These absorbing coating materials exhibited the highest maximum value of compressive residual stresses and the greatest depth of penetration. The obtained data demonstrate that when aluminum foil or black paint is employed, approximately 10% of the energy is lost at the coating–sample boundary, which corresponds to a loss of almost 20% in terms of pulse amplitude. The PVC tape–sample boundary exhibited a low degree of permeability to the wave, resulting in the loss of up to 80% of the pulse amplitude.

From a technological point of view, the advantage of foil is the possibility of rapid application compared to black paint, which must be applied layer by layer, and its efficient use for parts with simple geometries. However, in the presence of small radii of curvature and a more complex geometry, there is a risk of loss of adhesion between the foil and the part, which can lead to the rupture of the protective layer or the formation of defects on the surface of the material in the area of discontinuities at the boundary of contact of the protective layer. In this instance, the application of paint is a more suitable option, although it necessitates a considerably longer period of time to achieve the required thickness of the protective layer.

The investigations revealed no discernible alterations in the microstructure morphology, despite the presence of considerable residual stresses, as determined by the hole drilling method. In particular, the rotation of alpha plates towards the plastic flow direction or the flattening of alpha grains was not observed. Additionally, there was no evidence of the intense formation of low-angle boundaries of deformation origin or twinning, and the associated microstructure refinement. Indeed, the observed microstructural alterations were constrained by comparatively modest contrast fluctuations in the IQ and KAM maps, indicating a correlation with an elevated dislocation density.

The morphology of the initial microstructure (lamellar or globular) did not significantly influence the microstructural processes during LSP. However, this effect may be an artifact due to the relatively low sensitivity of orientation microscopy to purely dislocation processes.

The microhardness analysis of the specimens along the depth also did not reveal any significant changes. The application of laser shock peening led to an increase in the microhardness of the material for all types of absorbing coating.

Thus, a comprehensive study of all the most commonly used absorbing coating materials, including the processing mode without an absorbing layer, was carried out in the work. The most suitable materials of these layers for LSP were identified, and the effect of laser treatment on the microstructure of the titanium alloy was studied.

Author Contributions: Conceptualization, O.P. and S.Z.; methodology, O.P., S.Z., E.G., D.D. and M.O.; software, D.D., E.G., S.M. and A.K.; validation M.O. and S.M.; formal analysis E.G., A.K. and M.O.; investigation, D.D., E.G., S.M., M.O. and A.K.; data curation, A.K., E.G., D.D. and S.M.; writing—original draft, E.G.; writing—review and editing, O.P., D.D. and S.Z.; visualization, D.D., A.K. and E.G.; supervision, O.P. and S.Z.; project administration, O.P. and S.Z. All authors have read and agreed to the published version of the manuscript.

Funding: This research was funded by Ministry of Science and Higher Education of the Russian Federation, agreement No. 075-15-2024-535 dated 23 April 2024.

Data Availability Statement: The raw data supporting the conclusions of this article will be made available by the authors on request.

Conflicts of Interest: The authors declare no conflicts of interest.

References

1. Clauer, A.H. Laser Shock Peening, the Path to Production by LSP Technologies. *Metals* **2019**, *9*, 626. [\[CrossRef\]](#)
2. Ge, M.Z.; Xiang, J.Y. Effect of laser shock peening on microstructure and fatigue crack growth rate of AZ31B magnesium alloy. *J. Alloys Compd.* **2016**, *680*, 544–552. [\[CrossRef\]](#)
3. Iziumova, A.; Zhelnin, M.Z.M.; Kostina, A.K.A.; Vshivkov, A.V.A.; Gachegova, E.G.E.; Plekhov, O.P.O.; Swaroop, S. Fatigue life investigation of notched TC4 specimens subjected to different patterns of laser shock peening. *Frat. Integr. Strutt.* **2023**, *17*, 100–111. [\[CrossRef\]](#)
4. Sun, R.; Keller, S.; Zhu, Y.; Guo, W.; Kashaev, N.; Klusemann, B. Experimental-numerical study of laser-shock-peening-induced retardation of fatigue crack propagation in Ti-17 titanium alloy. *Int. J. Fatigue* **2021**, *145*, 106081. [\[CrossRef\]](#)
5. Elango, K.; Hoppus, J.S.; Kukreja, L.M.; Ostendorf, A.; Gurevich, E.L. Studies on ultra-short pulsed laser shock peening of stainless-steel in different confinement media. *Surf. Coat. Technol.* **2020**, *397*, 125988. [\[CrossRef\]](#)
6. Lim, H.; Lee, M.; Kim, P.; Park, J.; Jeong, S. Improvement of surface hardness of duplex stainless steel by laser shock hardening for the application to seawater desalination pump. *Desalin. Water Treat.* **2010**, *15*, 43–47. [\[CrossRef\]](#)
7. Jose, B.; Patil, T.; Rajan, S.S.; Praveenkumar, K.; Manivasagam, G.; Swaroop, S. Effect of laser shock peening without coating (LPwC) on a surface and sub-surface characteristics of aged Ti 15 V-3Al-3Cr-3Sn alloy. *Mater. Today Proc.* **2021**, *46*, 578–582. [\[CrossRef\]](#)
8. Maharjan, N.; Ramesh, T.; Wang, Z. High energy laser shock peening of Ti6Al4V alloy without any protective coating. *Appl. Surf. Sci.* **2023**, *638*, 158110. [\[CrossRef\]](#)
9. Correa, C.; Peral, D.; Porro, J.A.; Díaz, M.; De Lara, L.R.; García-Beltrán, A.; Ocaña, J.L. Random-type scanning patterns in laser shock peening without absorbing coating in 2024-T351 Al alloy: A solution to reduce residual stress anisotropy. *Opt. Laser Technol.* **2015**, *73*, 179–187. [\[CrossRef\]](#)
10. Lan, L.; Jin, X.; Gao, S.; He, B.; Rong, Y. Microstructural evolution and stress state related to mechanical properties of electron beam melted Ti-6Al-4V alloy modified by laser shock peening. *J. Mater. Sci. Technol.* **2020**, *50*, 153–161. [\[CrossRef\]](#)
11. Maruschak, P.; Menou, A.; Czausow, M.; Mocharskyi, V. Fractographic analysis of surface and failure mechanisms of nanotitanium after laser shock-wave treatment. *Key Eng. Mater.* **2014**, *592*, 346–349. [\[CrossRef\]](#)
12. Lan, L.; Xin, R.; Jin, X.; Gao, S.; He, B.; Rong, Y.; Min, N. Effects of laser shock peening on microstructure and properties of Ti-6Al-4V titanium alloy fabricated via selective laser melting. *Materials* **2020**, *13*, 3261. [\[CrossRef\]](#) [\[PubMed\]](#)
13. Jin, X.; Lan, L.; Gao, S.; He, B.; Rong, Y. Effects of laser shock peening on microstructure and fatigue behavior of Ti-6Al-4V alloy fabricated via electron beam melting. *Mater. Sci. Eng. A* **2020**, *780*, 139199. [\[CrossRef\]](#)
14. Zhou, W.; Ren, X.; Liu, F.; Ren, Y.; Li, L. Nanocrystallization in the duplex Ti-6Al-4V alloy processed by multiple laser shock peening. *Metals* **2016**, *6*, 297. [\[CrossRef\]](#)
15. Pan, X.; He, W.; Huang, X.; Wang, X.; Shi, X.; Jia, W.; Zhou, L. Plastic deformation behavior of titanium alloy by warm laser shock peening: Microstructure evolution and mechanical properties. *Surf. Coat. Technol.* **2021**, *405*, 126670. [\[CrossRef\]](#)
16. Altenberger, I.; Nalla, R.K.; Sano, Y.; Wagner, L.; Ritchie, R.O. On the effect of deep-rolling and laser-peening on the stress-controlled low- and high-cycle fatigue behavior of Ti-6Al-4V at elevated temperatures up to 550 °C. *Int. J. Fatig.* **2012**, *44*, 292–302. [\[CrossRef\]](#)
17. Zhang, X.C.; Zhang, Y.K.; Lu, J.Z.; Xuan, F.Z.; Wang, Z.D.; Tu, S.T. Improvement of fatigue life of Ti-6Al-4V alloy by laser shock peening. *Mater. Sci. Eng. A* **2010**, *527*, 3411–3415. [\[CrossRef\]](#)
18. Lu, H.; Wang, Z.; Cai, J.; Xu, X.; Luo, K.; Wu, L.; Lu, J. Effects of laser shock peening on the hot corrosion behaviour of the selective laser melted Ti6Al4V titanium alloy. *Corr. Sci.* **2021**, *188*, 109558. [\[CrossRef\]](#)

19. Altenberger, I.; Stach, E.; Liu, G.; Nalla, R.; Ritchie, R. An in situ transmission electron microscope study of the thermal stability of near-surface microstructures induced by deep rolling and laser-shock peening. *Scr. Mater.* **2003**, *48*, 1593–1598. [[CrossRef](#)]
20. Clauer, A.H.; Lahrman, D.F. Laser shock processing as a surface enhancement process. *Key Eng. Mater.* **2001**, *197*, 121–144. [[CrossRef](#)]
21. Ren, X.D.; Zhou, W.F.; Liu, F.F.; Ren, Y.P.; Yuan, S.Q.; Ren, N.F.; Xu, S.D.; Yang, T. Microstructure evolution and grain refinement of Ti-6Al-4V alloy by laser shock processing. *App. Surf. Sci.* **2016**, *363*, 44–49. [[CrossRef](#)]
22. Humphreys, F.J. Review grain and subgrain characterisation by electron backscatter diffraction. *J. Mater. Sci.* **2001**, *36*, 3833–3854. [[CrossRef](#)]
23. Íris, C.; Simões, S. Recent advances in EBSD characterization of metals. *Metals* **2020**, *10*, 1097. [[CrossRef](#)]
24. Schwartz, A.J.; Kumar, M.; Adams, B.L.; Field, D.P. (Eds.) *Electron Backscatter Diffraction in Materials Science*; Springer: New York, NY, USA, 2009; Volume 2, pp. 2–9.
25. Field, D.P. Recent advances in the application of orientation imaging. *Ultramicroscopy* **1997**, *67*, 1–9. [[CrossRef](#)]
26. *ASTM E837-13a*; Standard Test Method for Determining Residual Stresses by the Hole-Drilling Strain-Gage Method. ASTM International: West Conshohocken, PA, USA, 2013.
27. Schajer, G.S. Measurement of Non-Uniform Residual Stresses Using the Hole-Drilling Method. Part I—Stress Calculation Procedures. *J. Eng. Mater. Technol.* **1988**, *110*, 338–343. [[CrossRef](#)]
28. Corrêa, F.J.; Jahnert, F.A.; Tomás, J.P. Residual stress profile determination by the hole-drilling method with calibration coefficients obtained using FEM. *J. Theor. Appl. Mech.* **2021**, *59*, 661–673. [[CrossRef](#)]
29. Documentation for Hardness Testers of the Production Company “METOLAB”/Founder of METOLAB.—Moscow. 2023. Available online: <https://metolab.ru/dokumentaciya> (accessed on 5 June 2024).
30. Borisova, E.A.; Bochvar, G.A.; Brun, M.Y. Titanium alloys: Metallography of titanium alloys. In *Metallurgy*; Publisher: Moscow, Russia, 1980; p. 464.
31. Ashby, M.F. The deformation of plastically non-homogeneous materials. *Philos. Mag.* **1970**, *21*, 399–424. [[CrossRef](#)]
32. Fabbro, R.; Fournier, J.; Ballard, P.; Devaux, D.; Virmont, J. Physical study of laser-produced plasma in confined geometry. *J. Appl. Phys.* **1990**, *68*, 775–784. [[CrossRef](#)]

Disclaimer/Publisher’s Note: The statements, opinions and data contained in all publications are solely those of the individual author(s) and contributor(s) and not of MDPI and/or the editor(s). MDPI and/or the editor(s) disclaim responsibility for any injury to people or property resulting from any ideas, methods, instructions or products referred to in the content.